P-20

MULTIPLE SENSOR SMART ROBOT HAND WITH FORCE CONTROL

Richard R. Killion
Lee R. Robinson
Antal Bejczy

JET PROPULSION LABORATORY
California Institute of Technology
Pasadena, California

I. INTRODUCTION

Analysis of anticipated space assembly, servicing and repair tasks to be performed by robot arms motivated the work at the Jet Propulsion Laboratory (JPL) for the design and development of multifunctional and smart robot hands. Here the term "multifunctional" refers to the hand's mechanical capabilities, while the term "smart" refers to the hand's sensing and control capabilities. The analysis also led to the conclusion that an evolutionary approach to the design and development of robot hands can generate important and needed capability increases. The first step in this evolutionary development effort was the consideration of one degree-of-freedom parallel claw end effectors equipped with force/torque balance and grasp force sensors, and capable of being servoed in position, rate, and grasp force modes of control.

This paper describes a smart robot hand developed at JPL for the Protoflight Manipulator Arm (PFMA) at the Marshall Space Flight Center (MSFC). The development of this smart hand was based on an integrated design and subsystem architecture by considering mechanism, electronics, sensing, control, display and operator interface in an integrated design approach. The mechanical details of this smart hand and the overall subsystem integration are described elsewhere (Refs. 1 and 2). In this paper we briefly summarize the sensing and electronics components of the JPL/PFMA smart hand and describe in some detail its control capabilities.

II. THE MECHANICAL HAND

II.1 Requirements

The smart hand was designed for and integrated with the PFMA to perform the following specific tasks:

Task 1: Mate and demate a standard fluid coupling.

Task 2: Open and close an access panel by turning a wing nut.

Task 3: Remove and replace a battery module by grasping a square beam.

Task 4: Deploy and retrieve a telescoping vertical antenna.

The gripper's intermeshing claws were designed to grasp square beams (as attached in Orbital Replacement Units) as well as round and oval beams. In addition, a graphics display subsystem provides sensor information to the human operator during task performance. Figure 1 shows the mechanism of the end effector and the overall integrated subsystem including electronics, data handling, display and control input panel.

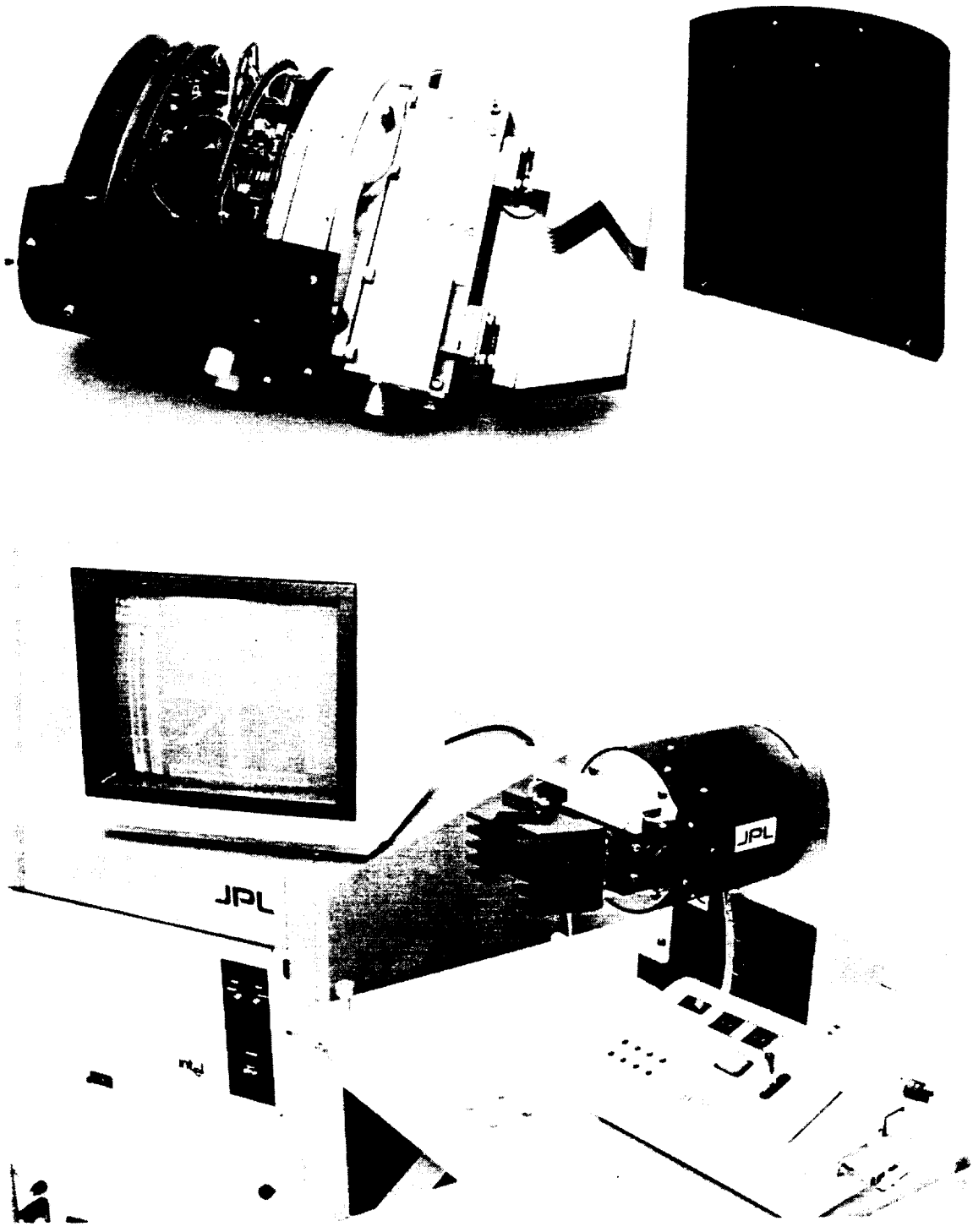

Figure 1. PFMA/JPL Smart End Effector Mechanism, Local Electronics and Overall Subsystem

III. SMART HAND SENSORS

III.1 F/T sensor

During the grasping phase in a zero-g environment, unwanted forces and torques can be detrimental to both the success of the task and the satellite being serviced. To monitor such forces and torques, a force/torque sensor is mounted between the hand and wrist. Semiconductor strain guages are mounted in the Maltese Cross design force/torque sensor with a full-bridge configuration. This configuration results in eight analog guage readings that are read and converted to 12-bit digital values by the Sensor CPU for eventual display for the human operator.

III.2 Clamping Force Sensor

Mounted in the base of each of the two fingers are four semiconductor strain guages in a full bridge configuration. They have been designed to measure up to 120 pounds of clamping force. These readings are converted to 12-bit digital by both the Sensor CPU and Servo CPU. The Servo CPU requires the digitized sensor data in real-time (400 hz) for servoing. The Sensor CPU requires the sensor data to be sent to the Signal Processing CPU for the slower (30 hz) graphics display.

III.3 Tachometer and Potentiometer

Rate and position information is required by the Servo CPU for motor control of the hand closure. Position information is required by the Sensor CPU for eventual display for the human operator.

III.4 Tactile Sensing

For future use, there is a reserve of 32 additional analog channels for force sensing of each of the individual plates of the intermeshing fingers. The force profile along the plates will give misalignment information to reduce torque applied to satellites in a zero-g environment.

III.5 Optical Proximity Sensing

Future plans also include optical proximity sensing. A proximity sensor consists of a photoemitter and a photodector with are focused such that the optic axes of the two converge at a focal point. Distance is determined by the intensity of the light received by the photodetector. This will reduce misalignment before contact, thus reducing unwanted forces and torques during contact.

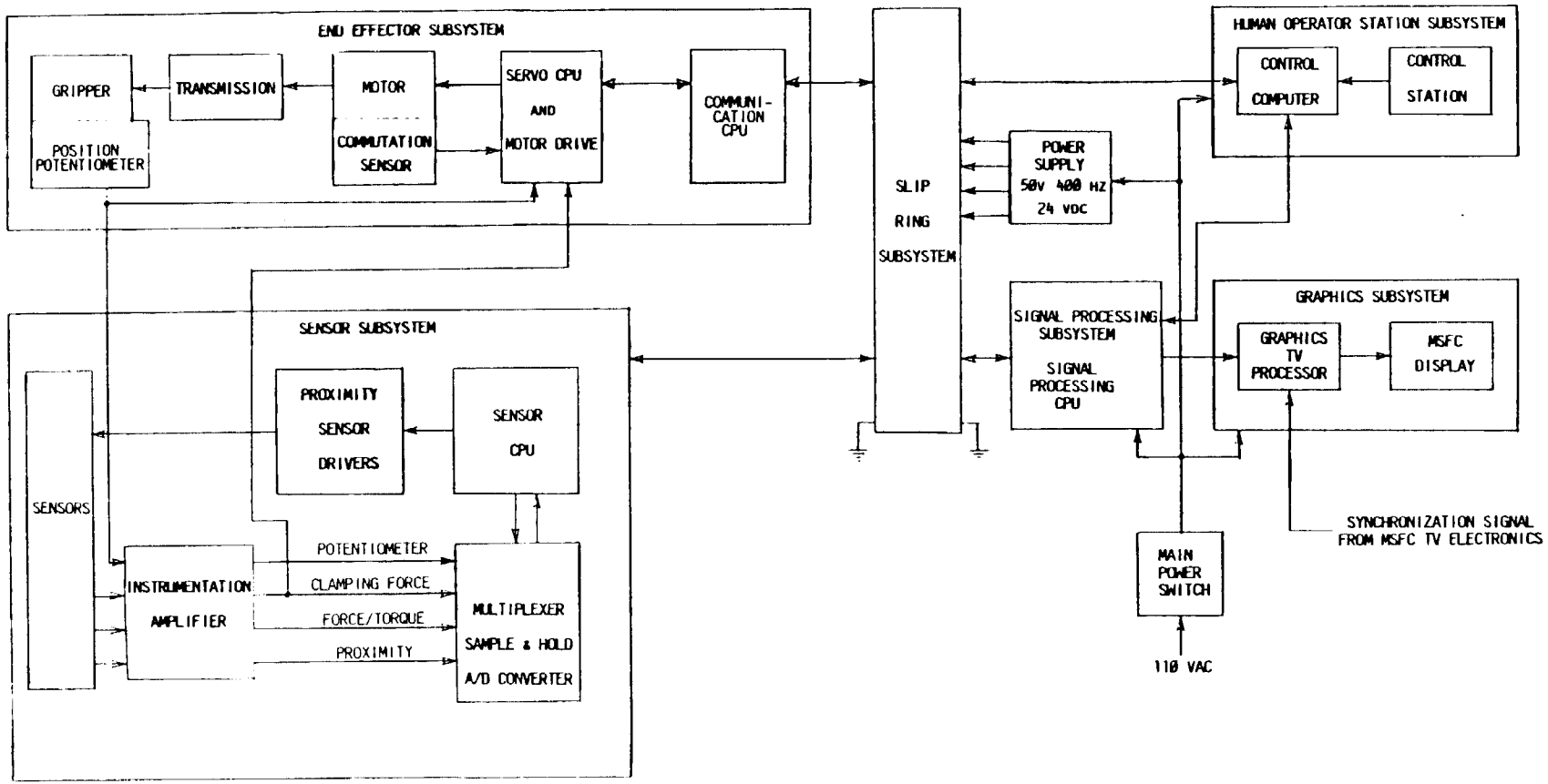

Figure 2. Overall Data Handling for PFMA/JPL Smart Hand

IV. LOCAL ELECTRONICS

The local electronics (electronics in the base of the hand) consists of the Sensor Subsystem and the End Effector Subsystem. See Figure 2.

IV.1 Sensor Subsystem

The Sensor Subsystem consists of the Sensor CPU, Multiplexer, Sample & Hold, A/D converter and instrumentation amplifiers. The Sensor CPU controls the analog multiplexing and the A/D conversion. The multiplexer handles 8 force/torque channels, 2 clamp force channels, and 1 position channel. After the Sensor CPU receives a conversion complete signal, it reads in the data and transmits it on request to the Signal Processing Subsystem via an RS-232 serial link through the Slip Rings.

IV.2 End Effector Subsystem

The End Effector Subsystem constists of two CPUs, the Motorola MC68701 for communications and the Motorola MC68705 for motor servoing.

The Communication CPU receives commands from the Control Computer in the Human Operator Subsystem via an RS-232 serial link through the slip rings. It receives serial data through its on-chip serial port and then checks for transmission errors using a 16-bit checksum. If the command is error-free, it passes the command to the Servo CPU via fast (30 micro seconds) parallel communication.

The Servo CPU executes the command to control the 3-phase D.C. brushless motor. Pulse width modulation and commutation to the motor windings is also done by the Servo CPU.

V. EXTERNAL ELECTRONICS

The External Electronics (electronics not in the hand) consist of the Slip Ring Subsystem, Human Operator Subsystem and the Graphics Subsystem. See figure 2.

V.1 Slip Ring Subsystem

The interface between the smart hand and the PFMA is a rotary slip ring joint. Seven slip ring connections were allocated for power (24 VDC & 20khz 50 VAC), and data communications for both the Sensor Subsystem and End Effector Subsystem.

V.2 Hperator Subsystem

rt of the test system, and also as an independent input ce to the smart hand besides the MSFC Control Compui Control Box was developed. This Control Box has a joys(1-degree of freedom), a slide switch(to command positi 3-way toggle switch (to switch modes), 2 rotary dial hes,(to set rate and force limits), a "hold" buttord status display "LEDs". This box has a Control Computhich is a Motorola MC68705. The joystick, along with ode,clamping force limit and rate limit switches is reathe MC68705. The proper command is generated and sent he Communication CPU via RS-232 across the slip rings e Communication CPU.

V.3 SiProcessing Subsystem

Tignal Processing CPU reads the sensor data from the R serial data stream coming from the Sensor CPU. It thends graphics commands via its Multibus to the Graphiocessor in the Graphics Subsystem.

V.4 Grs Subsystem

Traphics processor receives graphics commands from the 1 Processing CPU and generates a graphical represion of the force/torque, claw position, and clampirce. In figure 3 the three-axis coordinate system on thehics display shows the resultant forces. The bar graphsng the periphery of the display shows the resultorques due to roll, pitch and yaw. The vertical bars o left indicate gripper opening and clamping force sensedach of the two claws.

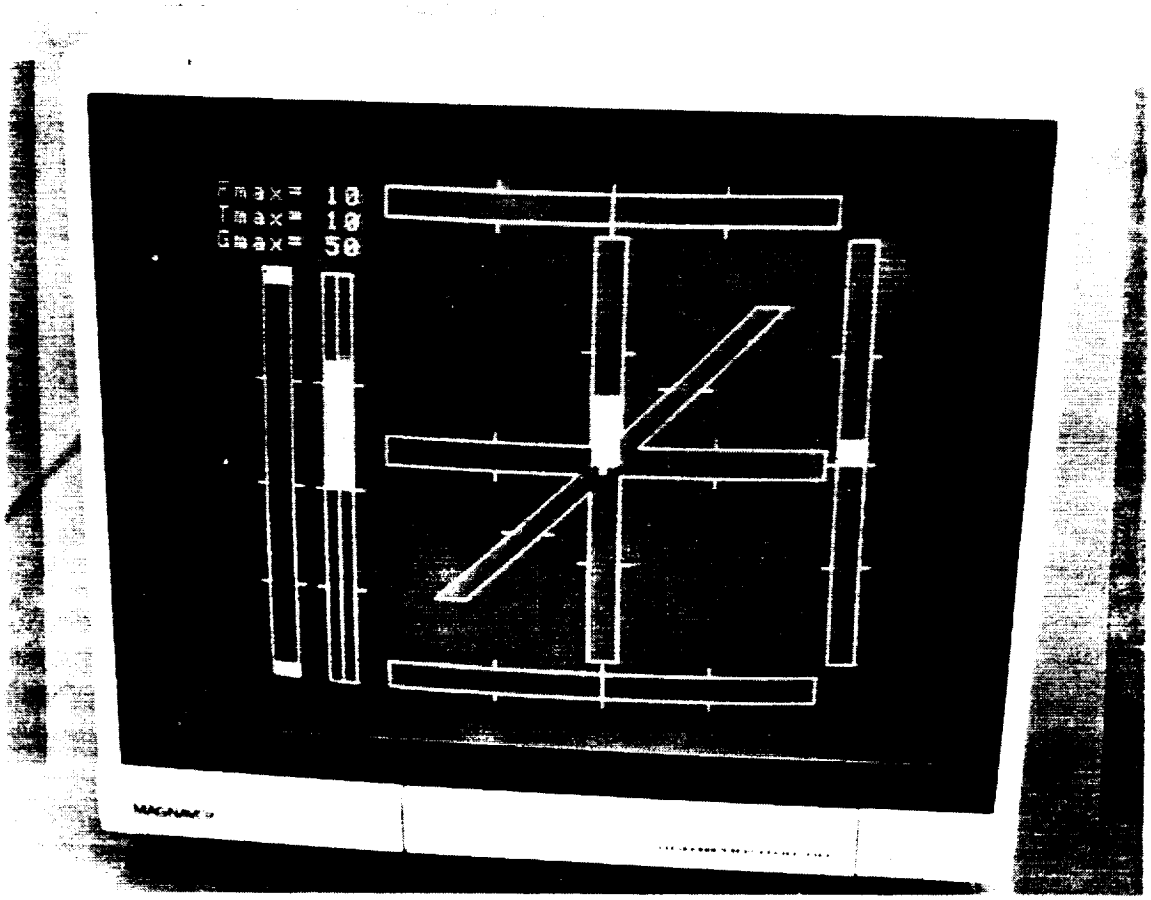

Figure 3. PFMA/JPL Smart End Effector Graphics Display (Left Vertical: e/e Opening-Closing Status; Second Vertical: Grasp Force Sensors Value; Center 2 and a 1/2 Frame: Up-Down, In-Out and Left-Right Forces; Top Horizontal: Roll Torque; Bottom Horizontal: Yaw Torque; Right Vertical: Pitch Torque)

VI. DESCRIPTION OF CONTROL MODES

Three primary control modes are designed into the smart hand. These modes are as follows:

(1) A Position Mode wherein the claws may be positioned to a specified differential opening and which incorporates an autonomous default "backup" mode if a force is detected. The hand reverses direction and stops after 1/8". It then refuses to accept position commands that would cause the same collision. This condition remains until the human operator either changes to rate mode or commands a position to move opposite the direction of the previous collision.

(2) A Rate Mode wherein the claws may be moved at a specified differential rate and which automatically transitions into a Force Mode Control configuration when an object has been encountered which generates a force opposing claw motion.

(3) A Hold Mode wherein a currently existing force which has been generated in Force Mode may be commanded to continuously control claw squeezing force without further command input.

A complete control mode diagram for the smart hand is shown in Figure 4. This diagram details the drive system hardware selected for the final system configuration. In addition, a computer simulation of this system has been generated for use in prediction of control mode performance. After optimizing the smart hand drive system hardware selection for motor torque-speed characteristics, power efficiency and feedback element resolution/dynamic range tradeoffs, consideration of algorithm parameters was undertaken.

The processor utilized as the smart hand servo controller is the Motorola MC68705 operating at 2MHz. It was considered imperative that all control algorithms (with attendent feedback data sampling) operate rapidly compared to the system response. A design target of less than 2.5 msec was considered desireable based upon the inherent need to minimize the buildup of force and energy transfer to the workpiece during conditions of unanticipated contact.

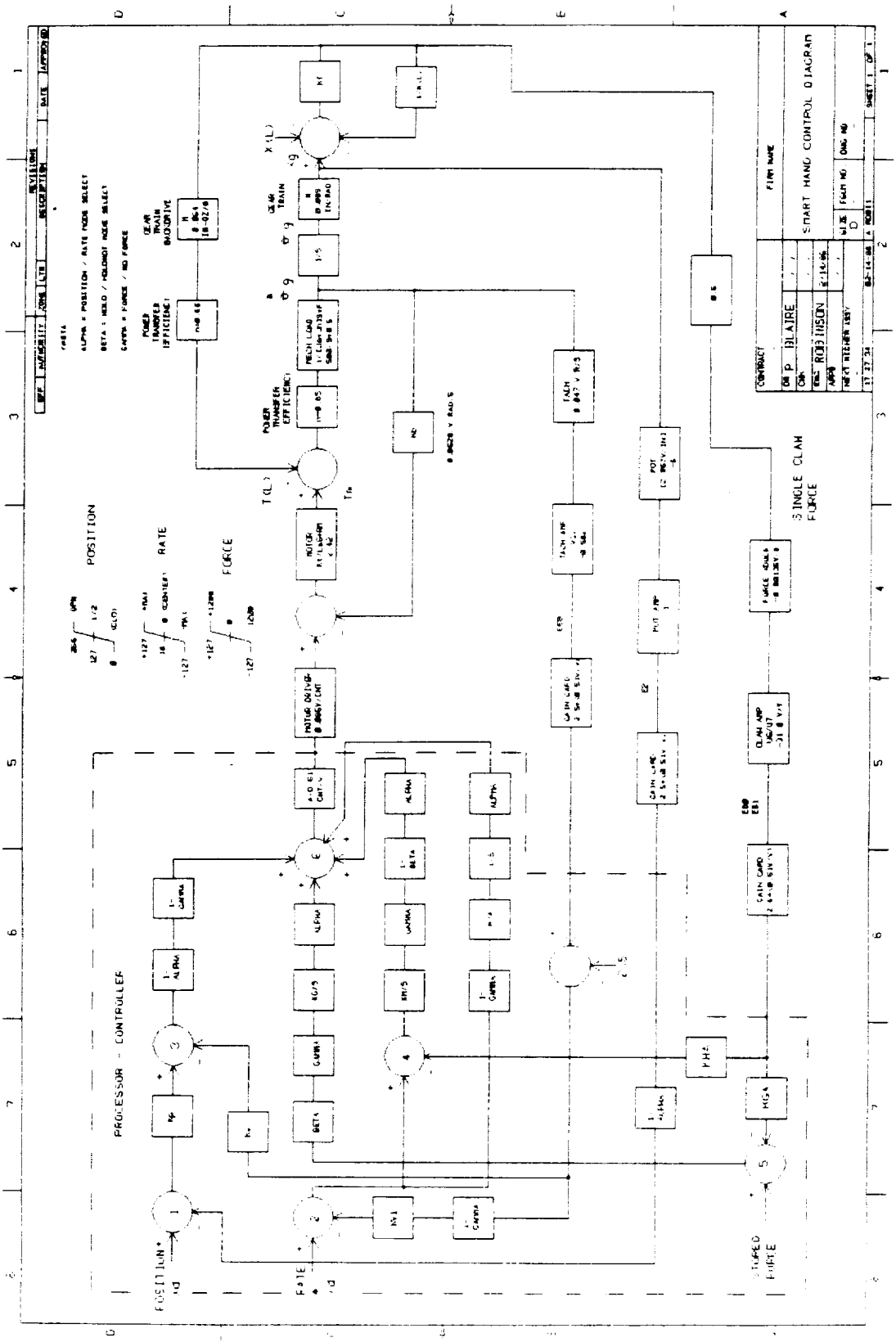

Figure 4. Smart Hand Control Diagram

VI.1 POSITION MODE

As can be determined from Figure 4, the Position loop has a characteristic equation of

$$s^2 + (42 + 42Kv)s + 36.3Kp.$$

Because the MC68705 processor being utilized has no hardware multiply/divide capability, it was desireable to implement algorithm gain factors as powers of 2 so that digital shift techniques could be utilized. Therefore, desiring a critically damped system, a set of appropriate gains would be Kv=0.25 and Kp=38. To incorporate digital shifts gains of Kv=0.25 and Kp=32 were selected. With data sampling at a 400 Hz rate and a control loop natural frequency of approximately 6 Hz, linear analysis should be applicable.

Four included figures document the expected and actual performance of the smart hand in Position mode. Figure 5 is the result of a simulation run using the analytically established gains, and shows slight overshoot. Figure 6 shows the results of a large position step test of the hand using the established gains. Slightly more overshoot is observed, however, this anomaly was traced to excessive mechanical deadband in the test unit which could not be readily remedied. In order to reduce the mechanical wear of the drive mechanism during testing, the gain Kp was reduced to 8. In addition, the rate feedback gain Kv was made position dependent, increasing to 0.5 when the actual position was within .100 inches of the commanded position. The performance with these changes is shown in Figure 7. Even though the position loop static accuracy was compromised by the gain reduction the increased smoothness of operation indicated overall increased benefits. Figure 8 indicates the large step position performance where an object is encountered prior to reaching the commanded position. As can be seen when a force is detected the claws stop trying to finish positioning and "back up" slightly to eliminate any detection of force and the hand awaits a subsequent valid command recognizing that it cannot complete the last one received.

VI.2 RATE MODE and RATE TO FORCE TRANSITION MODE

The Rate Mode configuration from Figure 4 yields a characteristic equation of

$$s^2 + 42s + 42Kva*Kv1.$$

Selecting Kva=8 and Kv1=1 as a proper gain set for the loop constants, provides an adequately damped system response as demonstrated by the simulator run output shown in Figure 9. System tests have validated these gain constants through demonstration of proper rate loop performance over the full dynamic range of operation.

Now to the more difficult section of the design requirements, the Force Mode control loop and the transitioning to it from the Rate mode. Without some predictor capability (i.e. proximity sensing) it is important that the bandwidth of the Force loop be maximized so that unplanned force transients imparted to the workpiece are minimized. From Figure 4 it can be determined that the characteristic equation of the Force mode configuration is

$$s^3 + 42.08s^2 + 2672.4s + 3752Kh*Kha.$$

Selecting Kh=1 and Kha=0.5 yields factors of

$$(s + 0.7)(s^2 + 41.3s + 2642).$$

These factors indicate a slightly underdamped control response. A simulator run output using the selected parameters is shown in Figure 10. The response is considerably less damped than the linearized system equations would indicate, however, this has been determined to be due to a realistic motor power limit included in the simulation. To compensate for the effect of power limiting the damping was increased by raising Kha to 1. Operational testing of the smart hand in the Rate mode with Auto Transitioning to Force indicated that the increased damping was adequate. Photos showing performance in these control regimes are included as Figures 11 thru 13. These tests were run by starting with the claws completely open and giving a full rate close command with obstacles of various compliances set to interfere with the closing. Figure 11 shows the transitioning region when a spring loaded compliance of approximately .001 in/lb was used as the target workpiece. Figure 12 shows the transitioning when a

solid aluminum bar (compliance less than .00001 in/lb) was utilized as the workpiece. The observable stepping in the force profile of relatively non-compliant loads is a phenomena of the software integrator and the incremental nature of the pulse width modulation resolution. Figure 13 is an expansion of the initial transient of Figure 12 demonstrating the transient energy transfer of the claw dynamics to the workpiece under near worst case conditions.

VI.3 HOLD MODE

Figures 14 and 15 show simulated performance of the control system to load disturbances when in the Hold Mode. The gains of the loop were set to Kg=1 and Kga=1 based upon the evaluation of the Force Mode response as previously described.

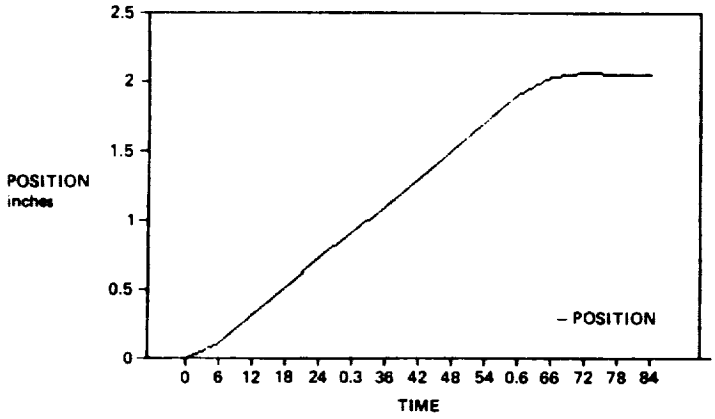

Figure 5. Smart Hand Position Mode

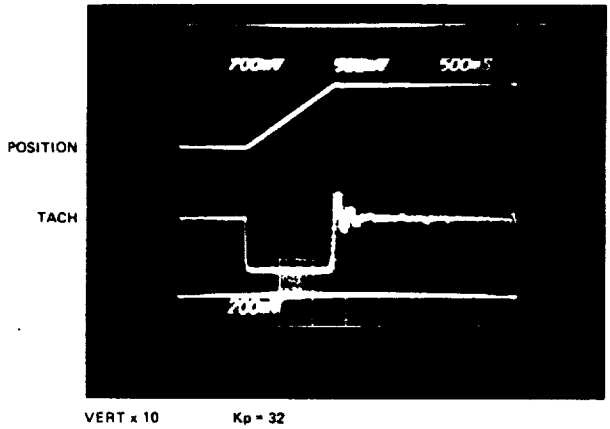

Figure 6. Position Servo Underdamped

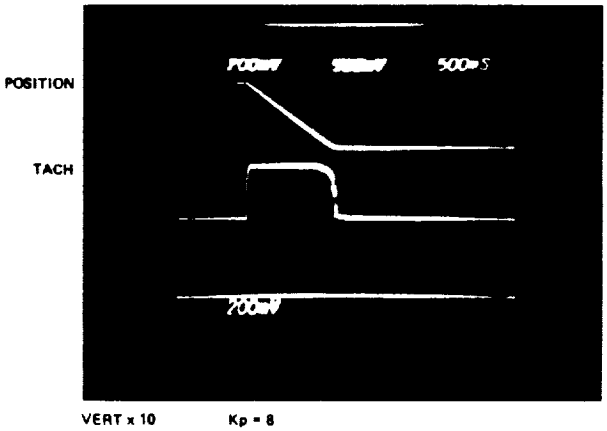

Figure 7. Position Servo Behavior

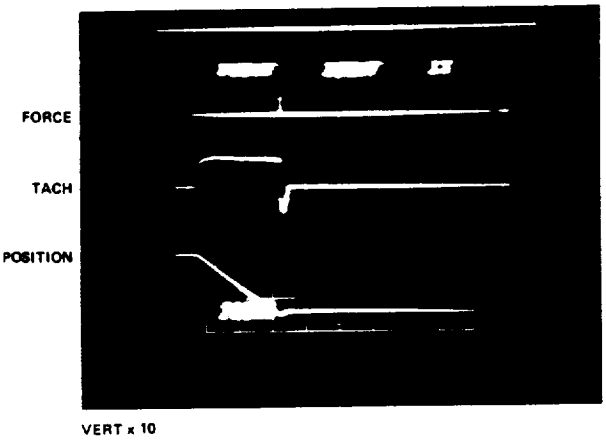

Figure 8. Position Mode With Interfering Force

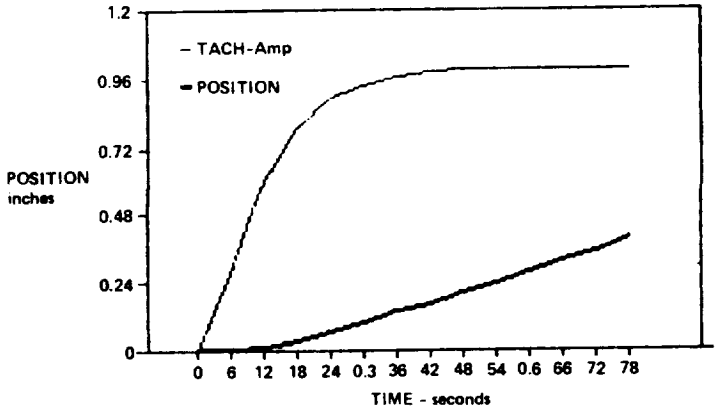

Figure 9. Smart Hand Rate Mode

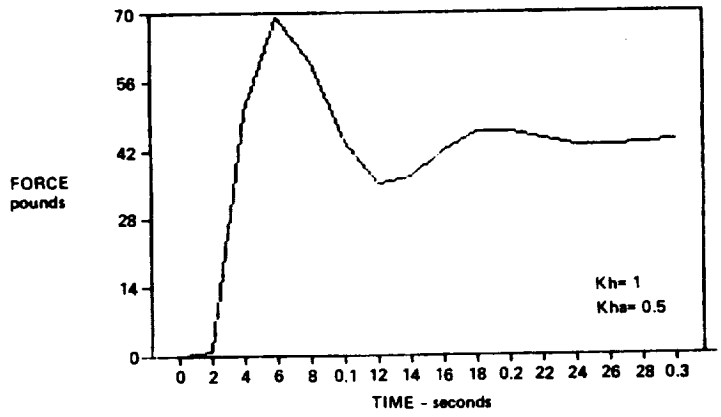

Figure 10. Smart Hand Force Without Hold

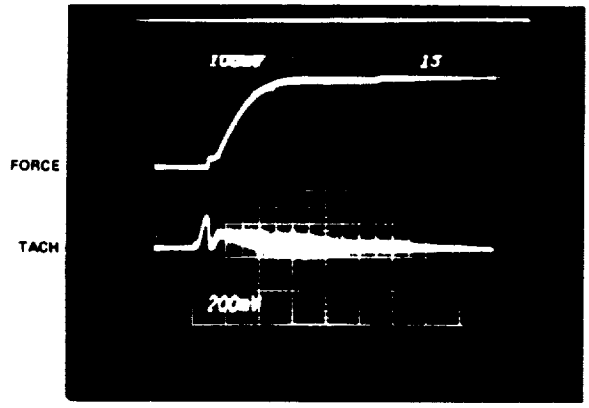

Figure 11. Rate to Force Transition - Full Rate

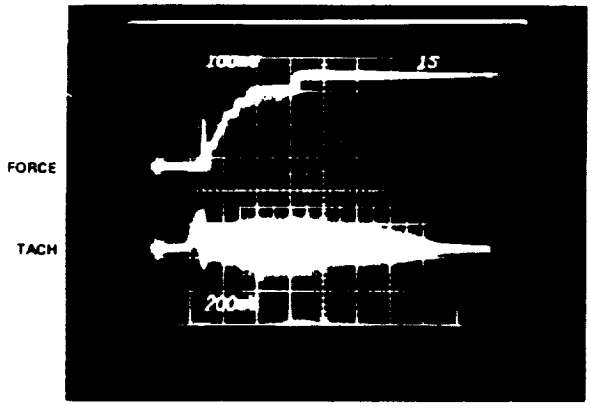

Figure 12. Rate to Force Transition - 1 sec/cm Scale

Figure 13. Rate to Force Transition - Full Rate Initial Transient Expanded 50 ms/cm Scale

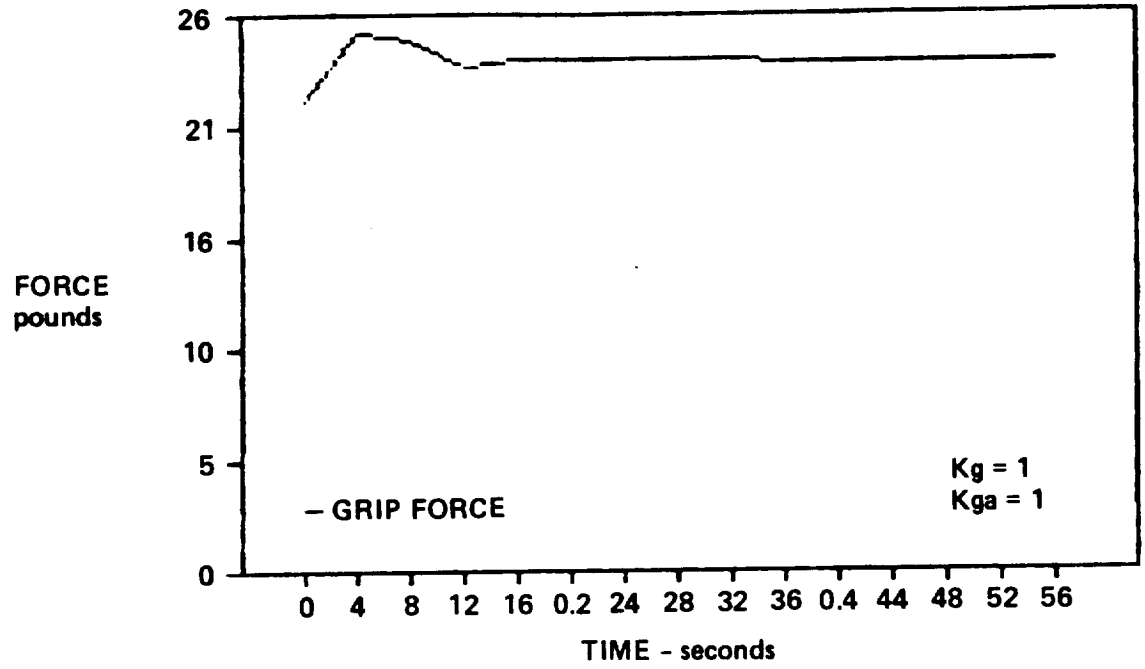

Figure 14. Smart Hand Force With Hold

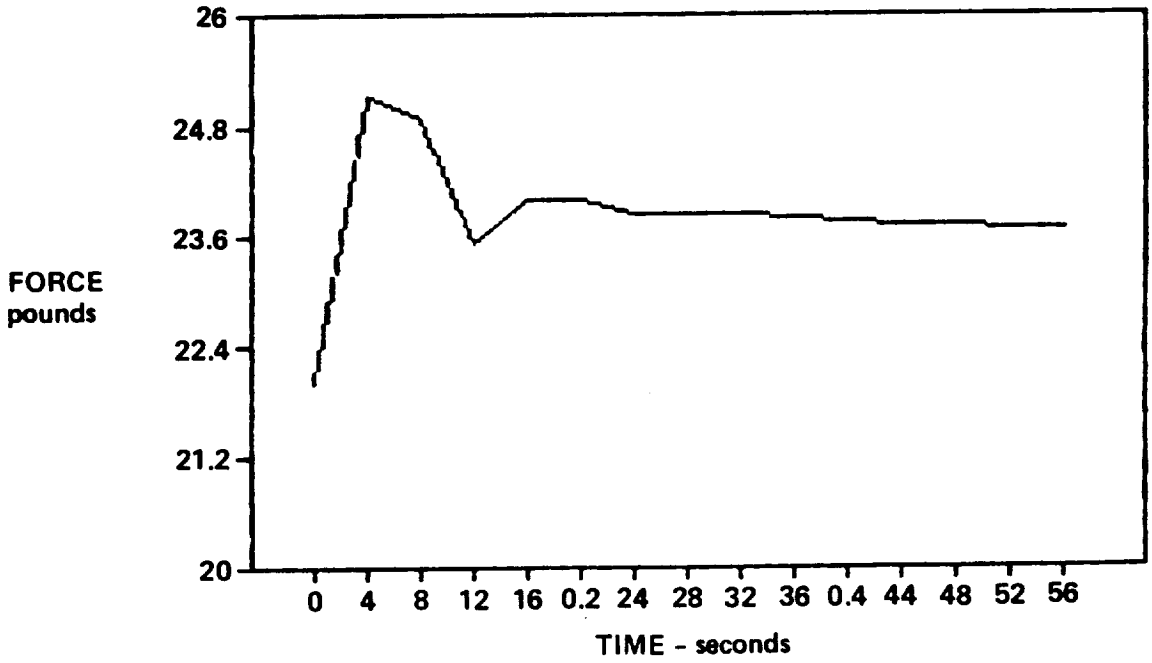

Figure 15. Smart Hand Force With Hold

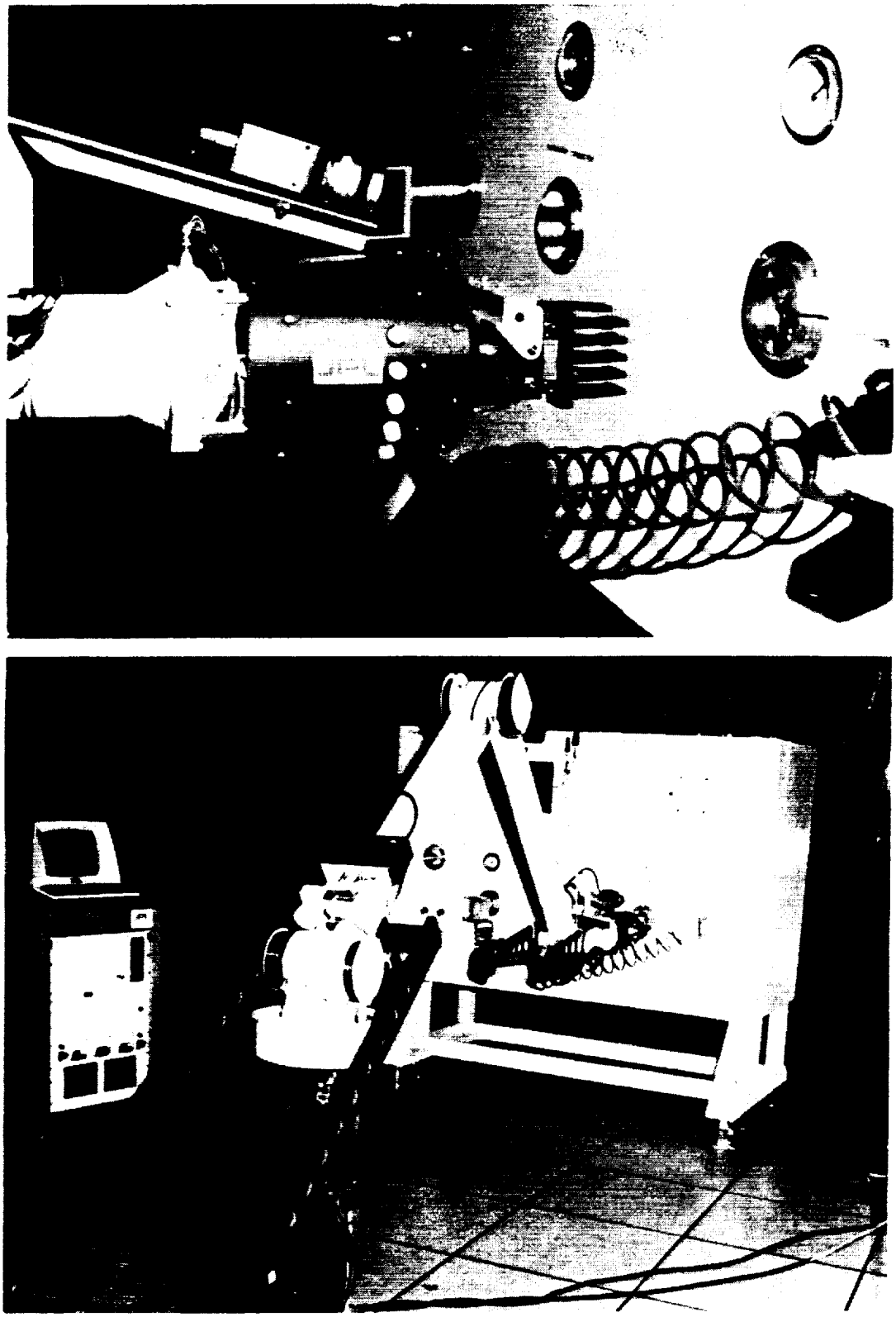

Figure 16. PFMA/JPL Smart End Effector Integrated With PFMA Arm at MSFC (Performing Connector Coupling Operation)

VII. CONCLUSION AND FUTURE PLANS

The smart hand has been mounted to the PFMA at MSFC (see Fig. 16) and tested with human operators performing simulated satellite servicing tasks. The tasks consisted of connecting and disconnecting a fluid coupling device, simulating module changeout, and attempting to exert constant forces and monents on the environment. Operators performed the tasks both with and without the force/torque display. Testing consisted of recording forces and torques from the wrist and jaw mounted sensors while operators performed tasks in manual control mode from a remotely located control station at MSFC. The tests and the results are described and evaluated in detail in Ref. 3.

In general, the experienced operators accomplished the tasks with lower levels of root-mean-square forces than intermediate or naive subjects. However, the test results have shown that improved display and manipulator control modes will be required to take full advantage of the end effector's sensing capabilities. The general conclusion is that sensors, displays, actuators and control modes for teleoperation cannot be designed or fully evaluated in isolation. For improved and optimized performance, the full teleoperation control loop, including the human operator, must be considered as it was pointed out in Ref. 3.

Future development plans include:

(i) Implementing the automatic execution of grasp force control

(ii) Implementing event driven displays

(iii) Designing a proximity ranging device integratable with the existing smart hand system.

In an event driven display, the simultaneous presence (or absence) of several force and torque component levels will be monitored and automatically indicated on the display with a distinct and easily perceivable symbol.

VIII. ACKNOWLEDGEMENT

This work was carried out at the Jet Propulsion Laboratory, California Institute of Technology, under contract to the National Aeronautics and Space Administration.

IX. REFERENCES

1. A.K. Bejczy and B.M. Jau, Servicing with Smart End Effectors on OMV Manipulator, Proceedings of Satellite Servicing Workshop II, Johnson Space Center, Houston, TX, November 6-8,1985.

2. A.K. Bejczy, E.P. Kan and R.R. Killion, Integrated Multi-Sensory Control of Space Robot Hand, AIAA Guidance, Navigation and Control Conference, Snowmass, CO, August 19-21,1985,paper no.: AIAA-85-1882.

3. B. Hannaford, Task Level Testing of the JPL-OMV Smart End Effector, Proceedings of Space Telerobotics Workshop, JPL-CALTECH, January 20-22,1987